Climate Dynamics (1995) 12:53–65

Climate Dynamics

Extratropical large-scale air-sea interaction in a coupled and uncoupled ocean-atmosphere model

Enda W. O'Brien and Eric P. Chassignet

RSMAS/MPO, University of Miami, 4600 Rickenbacker Causeway, Miami, FL 33149 USA

Received: 28 June 1994 /Accepted: 15 June 1995

Abstract. Spatial patterns of mid-latitude large-scale ocean-atmosphere interaction on monthly to seasonal time scales have been observed to exhibit a similar structure in both the North Pacific and North Atlantic basins. These patterns have been interpreted as a generic oceanic response to surface wind anomalies, whereby the anomalous winds give rise to corresponding anomalous regions of surface heat flux and consequent oceanic cooling. This mechanistic concept is investigated in this study using numerical models of a global atmosphere and a mid-latitude ocean basin (nominally the Atlantic). The models were run in both coupled and uncoupled mode. Model output was used to generate multi-year time series of monthly mean fields. Empirical orthogonal function (EOF) and singular value decomposition (SVD) analyses were then used to obtain the principal patterns of variability in heat flux, air temperature, wind speed, and sea surface temperature (SST), and to determine the relationships among these variables. SVD analysis indicates that the turbulent heat flux from the ocean to the atmosphere is primarily controlled by the surface scalar wind speed, and to a lesser extent by air temperature and SST. The principal patterns of air-sea interaction are closely analogous to those found in observational data. In the atmosphere, the pattern consists of a simultaneous strengthening (or weakening) of the mid-latitude westerlies and the easterly trades. In the ocean there is cooling (warming) under the anomalously strong (weak) westerlies and trade winds, with a weaker warming (cooling) in the region separating the westerly and easterly wind regimes. These patterns occur in both coupled and uncoupled models and the primary influence of the coupling is in localizing the interaction patterns. The oceanic patterns can be explained by the principal patterns of surface heat flux and the attendant warming or cooling of the ocean mixed layer.

Correspondence to: E. W. O'Brien

1 Introduction

Observational studies of large-scale extratropical air-sea interactions have found strong statistical links between the principal patterns of variability in the atmosphere and the principal patterns of variability in the northern oceans. Studies of this kind date back to Bjerknes (1964); a comprehensive review is provided by Frankignoul (1985). Representative recent papers are by Lanzante (1984), Wallace et al. (1990, 1992), and Cayan (1992a, b). In particular, Wallace et al. (1990, 1992) (hereafter WSJ and WSB, respectively) found that the principal patterns of *covariability* between sea surface temperature (SST) and atmospheric geopotential height had strong projections onto the dominant empirical orthogonal function (EOF) patterns from each domain separately. Indeed, the principal EOF patterns of each atmospheric and oceanic field were interpreted as patterns of large-scale atmosphere-ocean interaction.

Although weaker than the tropical EI Nino-Southern Oscillation phenomenon, extratropical air-sea interactions remain of considerable practical interest. Namias and Cayan (1981), Namias et al. (1988) and Palmer and Sun (1985), among others, found that extratropical SST anomalies had some value as predictors of European and North American climate on monthly to seasonal time scales.

The principal patterns of variability in the ocean and atmosphere do differ between the Atlantic and Pacific basins. However, as shown by WSJ, there is a striking similarity in the structure of the principal SST *tendency* pattern in each ocean, namely a relatively narrow strip of one polarity aligned zonally "sandwiched" between regions of opposite polarity to the north and south. Patterns of covariability between atmospheric and oceanic fields also show common features in each of the two basins.

In analyses of surface heat flux and its dependence on winds and air-sea temperature differences, Cayan (1992a, b) also found qualitative resemblance between the North Atlantic and Pacific oceans although, quanti-

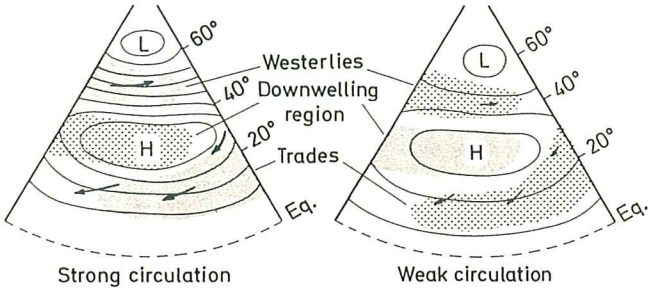

Fig. 1. Idealized depiction of sea-level pressure patterns, surface winds and anomalous SST tendencies observed during periods with negative (*left*) and positive (*right*) polarities of the principal western Atlantic and western Pacific atmospheric teleconnection patterns. *Fine dots* denote regions of cooling and *coarse dots* denote regions of warming relative to the climatological mean annual cycle in SST. (From Wallace et al. 1990)

tatively, the patterns in the two basins were quite different. Cayan (1992a, b) furthermore emphasized that the air-sea interaction patterns in both oceans were coherently organized on very large scales, and presented evidence that these patterns primarily represented atmospheric forcing of the ocean, a conclusion also reached by WSJ.

The observational evidence therefore suggests a simple schematic picture of how anomalous atmospheric circulations affect the ocean (Fig. 1). Atmospheric anomalies tend to fall into either high or low "index" circulations (Bjerknes 1964). The high index case corresponds to strong zonal westerlies in the westerly wind belt *and* strong easterlies in the trade wind belt. The low index case corresponds to weak westerlies *and* weak easterlies in their respective latitude belts. Associated with the high index circulation is an oceanic cooling tendency under the westerlies and the trades, with a warming tendency in the region in between. Tendencies are reversed in the low index case. While this qualitative scenario has been suggested by the observations, a premiss of our work is that further elucidation and validation can be provided by idealized models. To the best of our knowledge, this has not yet been performed.

In this study, large-scale air-sea interaction is therefore investigated in both uncoupled and coupled models of an extratropical ocean basin and a global atmosphere. The models are relatively idealized: the ocean basin has a rectangular box geometry, and zonally symmetric forcing is used for the atmosphere. Any patterns that emerge will thus be "generic", i.e., not specific to any particular ocean basin. However, the dimensions of the ocean are more representative of the North Atlantic than the North Pacific. The papers cited already provide the observational benchmark against which our results may be interpreted. The goals are to (1) quantify how much the turbulent heat fluxes across the air-sea interface are controlled by each of the relevant atmospheric and oceanic state variables; (2) extract the preferred patterns of air-sea interaction, and (3) identify those features that are due to one-way forcing of the ocean by the atmosphere and those that are due to the coupling. Linear relationships within and between atmospheric and oceanic fields are investigated using EOF and singular value decomposition (SVD) analyses.

Both coupled and uncoupled model versions are used in order to unambiguously determine how much of the air-sea "interaction" is really just atmospheric forcing of the ocean. In the uncoupled version synoptic variability in the atmosphere affects the ocean, but ocean variability (i.e., deviations from climatology) does not affect the atmosphere. The existence of large-scale coherent air-sea interaction patterns in the extratropics suggests that knowledge of one field might enhance predictability in the other. This was demonstrated by Miller and Roads (1990) in an uncoupled run where the mid-latitude ocean forced the atmosphere without being influenced by the atmosphere in return. In the coupled case, however, Miller and Roads (1990) showed that the atmospheric predictability was actually almost identical to the uncoupled case as the atmospheric errors gave rise to SST errors which in turn fed back onto the atmosphere. This feedback process can lead to a climate drift, as discussed by Manabe and Stouffer (1988) and Sausen et al. (1988). This has not been a problem for the results presented in this study.

The layout of the study is as follows: the individual oceanic and atmospheric models and the coupling procedure are described in section 2. The different climatologies of the uncoupled and coupled models are presented in section 3. The results of the SVD analysis of heat flux, SST, air temperature and wind speed variability are shown in section 4, along with results from a complementary EOF analysis. There is a concluding summary and discussion in section 5.

2 The coupled model

2.1 The ocean model

The oceanic component of the coupled model is a three-dimensional isopycnic coordinate model in a mid-latitude box domain from 10°N to 60°N, and 64° wide. The grid points form a regular 2° mesh on a Mercator projection, i.e., the north-south spacing of grid points changes with the spacing of meridians. The basic model is identical to that described by Bleck et al. (1989). In particular it has a mixed layer of the Kraus and Turner (1967) type, which overlies 5 isopycnal layers representing the stratified oceanic interior. Salinity is held constant. Forcing is provided by time- and space-dependent wind stress fields, radiative fluxes and turbulent heat fluxes. In Bleck et al. (1989), these are all specified as functions of latitude and time of year from observed climatologies. In the integrations described here only the radiative fluxes remain specified in this way; the rest are interactively determined from atmospheric model output. The (upward) turbulent heat flux H across the ocean surface is parameterized by:

$$H = c_D |\mathrm{v}| (SST - T_{Air}), \quad (1)$$

where c_D is a bulk coefficient, $|v|$ is the scalar surface windspeed, and T_{Air} is the air surface temperature. In the absence of variable salinity in the ocean and a moisture variable in the atmosphere, H is taken to represent both sensible and latent heat fluxes. This is achieved by allowing the air temperature T_{Air} in both uncoupled and coupled models to be lower than would be the case if H represented sensible heat fluxes only. The resulting heat flux then represents the combined sensible plus latent fluxes (Bleck et al. 1989). Since the ocean model is not eddy-resolving the nonlinear effects are small, and when forced by an atmospheric climatology the upper ocean circulation essentially repeats itself every year.

2.2 *The atmospheric model*

The atmospheric component of the coupled model is a conventional primitive equations, global spectral model run with two σ-layers in the vertical and an R15 horizontal truncation. For details on the model, the reader is referred to O'Brien et al. (1994). In the uncoupled mode, the external forcing is zonally symmetric (the lower boundary is flat). Forcing is provided by Newtonian relaxation to a specified "radiative equilibrium" temperature profile, which follows a simple seasonal cycle. The radiative time constant is 25 days. Surface friction is represented by Ekman pumping with a time scale of 9 days. No moist processes are represented in this model.

Even in uncoupled mode, internal instabilities and nonlinear interactions in the atmospheric model generate a rich spectrum of variability, and the model maintains a level of eddy kinetic energy comparable to that of the real atmosphere (see O'Brien et al. 1994).

2.3 *Coupling procedure*

The technique for coupling the atmospheric and oceanic models is simple in principle but complex in practice. The ocean model requires air surface temperature and wind data, which are provided by the atmospheric model at each oceanic time step. The atmospheric model in uncoupled mode requires no information from the ocean at all, but is forced by an idealized heating profile that *implicitly* includes a contribution from the ocean or land surface below each gridpoint. In coupled mode, this heating (or cooling) from the ocean is made explicit and is computed from the ocean model sea surface temperature.

Atmospheric output is computed on a Gaussian grid while the ocean model is solved on a Mercator grid, so data must be regularly and efficiently interpolated between them. Air surface temperatures are obtained by extrapolation from the lower layer temperatures and heights using a constant lapse rate of 5° C km^{-1}. Since surface friction acts on winds in the lower model layer, these winds are communicated to the ocean as surface winds. Coupling in time is synchronous; information is exchanged at each oceanic time step, which is three times as long as the atmospheric time step.

It is not realistic to simply insert the ocean model under the atmosphere and treat the resulting upward heat fluxes (on the order of 100 Wm^{-2}) as an additional forcing of the atmosphere. Rather, that part of the upward flux which is implicit in the default atmospheric forcing must be subtracted out first. The following procedure was used to identify that part of the forcing of the atmosphere which is due to the ocean: first, the atmosphere was run alone using its "standard" forcing functions. This run was used to generate a climatology of air surface temperatures and winds as functions of latitude and time of year. Second, these temperatures and winds were used to force the ocean model, also run alone. A climatology of ocean-to-atmosphere heat fluxes (as a function of latitude and time of year) was calculated from this integration, using the parameterization (1). These fluxes are interpreted as the implicit oceanic contribution to the atmospheric forcing when the atmosphere is run alone. When the models are coupled, these implicit climatological fluxes are subtracted from the full explicit fluxes calculated at each time step, and the residuals are used to force the atmosphere.

A forcing configuration was selected for the atmospheric model which reproduced as closely as possible the observed climatological surface wind and temperature fields over the North Atlantic, and the coupling procedure outlined was followed. The resulting sea surface temperature field was plausible at high latitudes but reached unrealistic values (over 50° C) in summer in the subtropics. To diagnose the cause, two sensitivity experiments were conducted: one with fixed winds and interactive temperatures, and the other with fixed temperatures and interactive winds. The high subtropical SSTs were determined to be due to weak trade winds in the atmospheric model. The strong easterly trades blowing along the southern flank of the Bermuda High are not simulated by the model because of its simplified physics. These winds appear to be crucial for transferring heat from the ocean to the atmosphere and keeping the SST within the observed range.

To compensate for this deficiency in the atmospheric model, the bulk parameterization scheme (1) was modified by adding an effective scalar wind speed correction, computed as the difference between the simulated windspeed climatology and the observed one from the Comprehensive Ocean-Atmosphere Data Set (COADS). The wind speed correction, shown in Fig. 2, is largest in summer in the subtropics. This correction is not a "flux correction" in the sense of Sausen et al. (1988), or as used by Manabe et al. (1991), since it is not only used in the coupled model but is needed in *both* coupled and uncoupled modes to compensate for systematic errors in the atmospheric component. The wind speed correction plays no role in the coupled model that it does not also play in the uncoupled models. Thus our coupled and uncoupled results can be compared directly without reference to this correction.

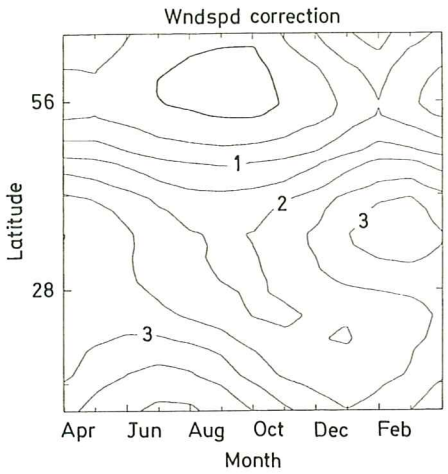

Fig. 2. Scalar wind speed correction added to lowest layer winds when calculating ocean-atmosphere heat fluxes. Contour interval is 0.5 ms^{-1}

2.4 Model integrations

Two model integrations are discussed in detail. The first one is the uncoupled case (henceforth the "U" case). Here the ocean is forced by the instantaneous atmospheric fields at each ocean time step, but the atmosphere only senses ocean climatology. The second integration is the fully coupled model (henceforth the "C" case). The models were integrated for 50 years in both cases. Only output from the last 30 years were used in the analyses described below. Ocean data were stored every 10 days and atmospheric data every day.

All the results presented here are based on time series of monthly mean fields, each 360 samples long, which were generated for all fields of interest. The atmospheric fields were also interpolated onto the oceanic grid which is necessary for computing quantities like heat flux. This also makes for simplicity and consistency in interpreting all interaction patterns.

3 Model climatology

In this section, we introduce the quantities that will be needed to address the issues raised in the introduction. First, we discuss the surface heat flux as it is the coupling mechanism common to both the atmosphere and ocean. The ocean is also forced by the two-dimensional atmospheric wind stress. We then describe the oceanic SST fields and atmospheric surface wind fields.

The seasonal cycle of zonally-averaged heat flux for the U and C cases is shown in Fig. 3. The seasonal cycle is defined by the 30-year average for each time of year at each gridpoint. Positive values are for upward-directed fluxes, and the values given are zonal averages across the basin for each latitude at each time of the year. The principal features and magnitudes are similar in both cases. There is a minimum at high latitudes in June, a maximum in January, and a minimum in the subtropics in October. Annual-mean heat flux fields for both U and C cases are shown in Fig. 4. They are again very similar, except for a small enhanced flux across the Gulf Stream in the C case. The seasonal cycle accounts for about 70% of the total domain-averaged standard deviation for all quantities in both U and C cases and, consequently, in the remainder of this study, the seasonal cycle has been removed before computing standard deviations in order to investigate variability independant of the seasonal cycle. Standard deviations of heat flux, with the seasonal cycle removed, for the U and C cases are then displayed in Fig. 5. There are significant differences between the two cases. In the U case, the atmospheric variability is zonally symmetric and variability in the heat flux is then rather incoherent. A weak maximum over the Gulf Stream reflects the influence of the SST. The decrease in variability toward the southern boundary reflects the lower wind speed variability there. In the C case, however, heat flux variability is concentrated over the western boundary current and over the southeastern part of the domain where the air temperatures (not shown) are especially variable. Heat flux variablity over the center of the ocean gyre is slightly reduced from the U case, as the air and ocean temperatures track each other in the C case.

Figure 6 shows the annual-mean SST and surface wind fields from the U and C cases. The fields in the C case have more zonal structure than in the U case, reflecting how the feedbacks in the coupling have established time-mean zonal asymmetries in the wind (and air temperature) fields as well as in the SST field. There is a mean southerly wind component over the western part of the ocean in the C case. This is also the case in observations (Hellerman and Rosenstein 1983) and is generally attributed to a standing wave pattern due to the presence of topography. Topography is, however, not present in our simulations.

The SSTs are slightly too warm at low latitudes in both model versions. This can be attributed to weaker than observed wind stresses generated by the atmospheric model. The error is not large enough, however, to warrant inclusion of a wind stress correction. We wish to keep the use of such corrections to a minimum, and the scalar wind *speed* correction described plays a much larger role in controlling SST. The latitudes of weak mean winds occur close to where they are found over the Atlantic and Pacific (Peixoto and Oort 1992).

Figure 7 shows standard deviations (without the seasonal cycle) of monthly-mean SST (contours) and surface winds (arrows) from the U and C cases. The eastward component of the arrows represent standard deviation of the u-component of the wind; the northward component of the arrows represent standard deviation of the v-component. Magnitudes are comparable in both cases, with more zonal structure in the C case, as expected.

4 Singular value decomposition

In this section, we would like to (1) quantify how much the turbulent heat fluxes across the air-sea interface

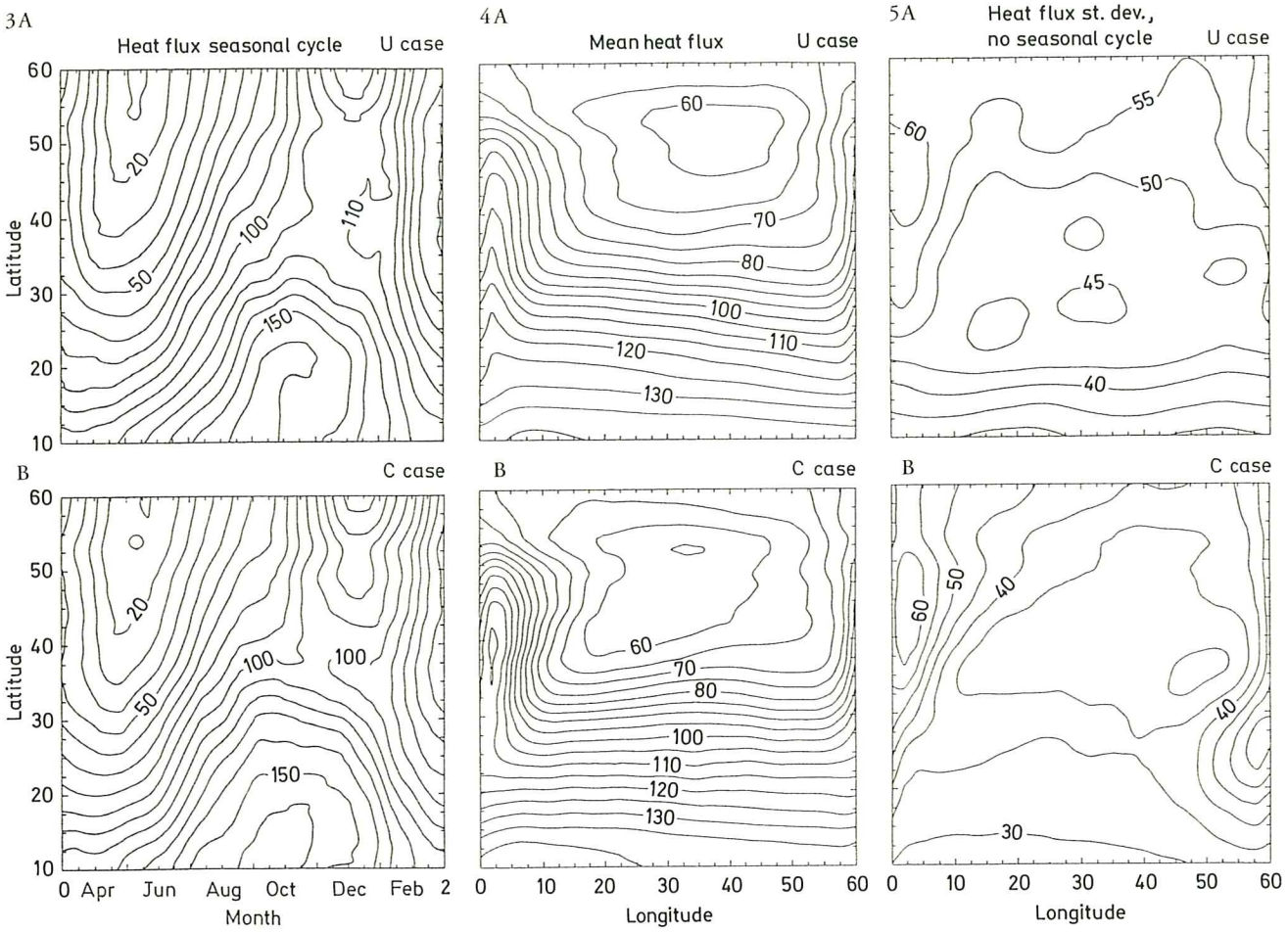

Fig. 3A, B. Seasonal cycle of zonally-averaged (upward) surface heat flux from **A** the U and **B** the C cases. Contour interval is 10 Wm^{-2}. Month "0" corresponds to March 15th

Fig. 4. A Annual mean surface heat flux fields from **A** the U and **B** the C cases. Contour interval is 10 Wm^{-2}

Fig. 5. A Standard deviations of surface heat flux, with the seasonal cycle removed, for **A** the U and **B** the C cases. Contour interval is 5 Wm^{-2}

are controlled by each of the relevant atmospheric and oceanic state variables; (2) extract the preferred patterns of air-sea interaction, and (3) identify those features that are due to one-way forcing of the ocean by the atmosphere and those that are due to the coupling. This is achieved by performing a thorough singular value decomposition (SVD) analysis on both the uncoupled (U) and coupled (C) model outputs.

Singular value decomposition (SVD) of the correlation or covariance matrix between two different fields is a statistical technique for identifying those pairs of spatial patterns that explain as much as possible of the mean-squared temporal correlation (or covariance) between the two fields. SVD modes are ordered according to how much of the squared correlation between two fields they explain, in the same way that EOF modes are ordered according to how much of the variance within a single field they explain. Bretherton et al. (1992) and WSB demonstrated that both in theory and in practice, SVD explains substantially more of the squared covariance between two different fields than other analysis techniques and is an efficient method for identifying linearly coupled modes between two different fields. The reader is referred to these two papers for a clear exposition of the technique and an evaluation of its performance. A mathematical summary of the technique is presented in the Appendix. In the interest of simplicity, and following WSB, we opt to show results based on correlations rather than covariances. Not surprisingly, the dominant mode of covariability between any two variables in the monthly mean data sets is the seasonal cycle. This mode is relatively uninteresting since its spatial patterns are virtually featureless. In the results shown next the seasonal cycle was therefore removed from all time series before computing the SVD.

4.1 SVD results for surface heat flux

In this subsection, we address the question of how much of the surface heat flux variability (as shown in Fig. 5B) can be accounted for by variability in each of the oceanic and atmospheric fields that contribute to it. SVD is used to find principal correlation patterns be-

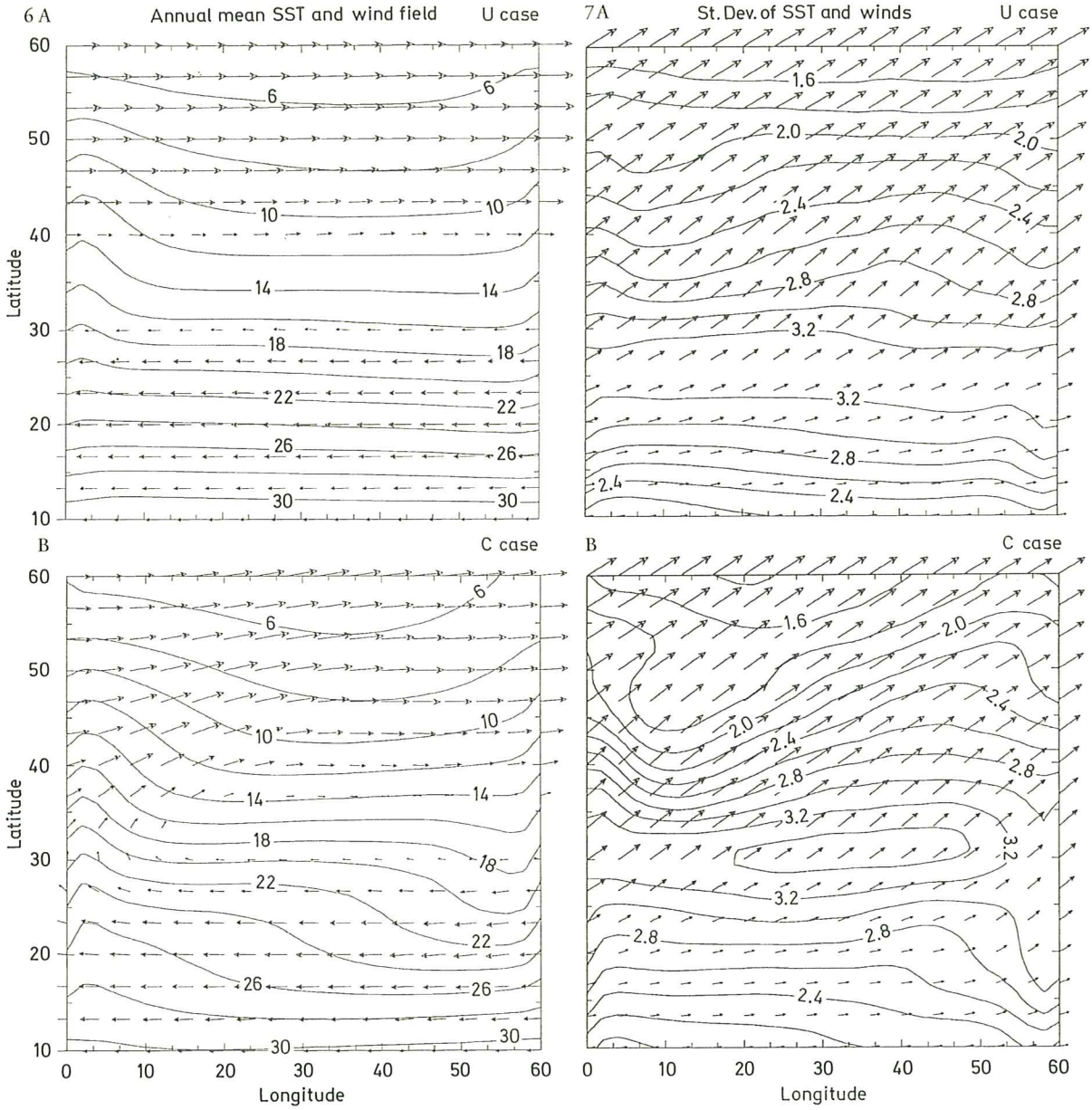

Fig. 6. A Annual mean SST and surface wind fields from the U and **B** the C cases. SST contours are every 2° C. *Maximum wind barbs* represent 5.6 ms^{-1} in **A** and 6.0 ms^{-1} in **B** winds weaker than 0.5 ms^{-1} are not shown

Fig. 7. A Standard deviations of SST and surface winds from **A** the U and **B** the C case, with the seasonal cycle removed. SST standard deviation contours are every 0.2° C. The *eastward* component of the wind barbs represents standard deviation of the *u*-component of the wind; the *northward* component represents standard deviation of the *v*-component. *Maximum wind barbs* correspond to 3.5 ms^{-1}

tween the surface heat flux and each of the following variables: SST, surface air temperature, $SST - T_{Air}$ surface windspeed and $d(SST)/dt$ (or SST tendency). SST tendency is defined here as the difference between mean SST for a given month and mean SST for the month before.

The quantitative SVD results using the monthly-mean time series from the U and C cases are summarized in Table 1. Numbers in the first two columns are the Frobenius norm ($\|C_{ST}\|_F^2$, see Appendix for a definition) of the correlation matrix between the heat flux field (the *S* field) and each of the other fields (the *T* field). They may be thought of as the root-mean-square correlation between each point in the heat flux field and each point in the other field and are naturally smaller than the average correlation between two fields at co-located points. These numbers show that surface heat flux is most strongly correlated with wind speed and most weakly correlated with SST, especially in the U case. Otherwise, the relationships between heat flux and the other fields are very similar in both U and C cases.

Table 1. SVD results for correlations between surface heat flux as one field (the S field) and SST, air temperature, SST minus T_{Air}, wind speed and SST tendency, respectively, as the other (the T field)

	$\|C_{ST}\|_F$		$\langle r(S, b_{1,2,6})^2 \rangle$	
	Uncoupled	Coupled	Uncoupled	Coupled
SST	0.09	0.13	2.6	4.8
			4.2	7.2
			7.1	12.2
T_{Air}	0.19	0.15	9.3	5.6
			16.9	10.4
			28.3	21.9
SST-T_{Air}	0.14	0.17	5.5	4.1
			9.4	8.2
			17.9	19.3
WIND	0.28	0.30	17.2	15.7
			27.5	30.0
			50.2	56.1
d(SST)/dt	0.15	0.15	5.0	6.4
			10.5	10.9
			17.83	18.6

Numbers in the first two columns are Frobenius norms of the correlation matrices (or rms correlations between points in the two fields). Numbers in the last two columns are area-averages (multiplied by 100) of squared correlations between the heat flux field and the first, the first two and the first six expansion coefficients of each of the other fields, respectively. The may be interpreted as percentage of the heat flux variance explained cumulatively by the first, the first two and the first six singular values of the other field, respectively. See text for further explanation

The second two columns in Table 1 show the cumulative percentage of heat flux variability explained by the first, the first two and the first six expansion coefficients (b_k, see Appendix for a definition) in the other field, respectively. For each mode k, this number is calculated by taking the spatial average of the square of the correlation between the heat flux field and the expansion coefficient b_k of that mode, or $<r(S, b_k)^2>$, where angle brackets denote a spatial average. Expansion coefficients, as defined in the Appendix, are analogous to expansion coefficients of EOFs. The first 6 SVD modes account for over 90% of all squared correlations for each case shown here. The first mode alone typically accounts for 30–40% of all squared correlations.

It can be seen from Table 1 that in the C case 4.8% of total heat flux variability can be explained by SST variability in mode 1, while 15.7% can be explained by wind speed variability in mode 1. Perhaps the more pertinent numbers in Table 1 are the bottom ones in columns 3 and 4 for each variable. These provide a measure of how well heat flux variability is explained by the first six expansion coefficients of each of the other four fields. Thus in the U case, SST variability accounts for about 7% of heat flux variance whereas wind speed variability accounts for over 50%.

The statistical significance of the SVD results may be estimated using a Monte Carlo data scrambling technique as in WSB and O'Brien et al. (1994). The order of months in one field are randomly scrambled and the SVD analysis repeated. Any "variance explained" can then be attributed to accident alone and a histogram of accidental "variance explained" can be constructed by applying SVD to many different scrambled time series. The significance of the results from *unscrambled* data can then be estimated by their position on the histogram. It was impractical to evaluate the statistical significance of all the numbers in Table 1. Instead, the singular values obtained by comparing the heat flux and SST tendency fields were selected for a comprehensive significance testing. The order of the heat flux timeseries was randomly scrambled 30 different ways, in both the U and C cases, and the SVD analysis was repeated each time. In comparison with these results, the results using unscrambled data were found to be highly significant, in the sense that less than 20% of the "variance explained" by the SVD patterns could be attributed to random chance. The significance of the remaining numbers in Table 1 was tested using only one scrambled trial instead of 30. This single trial suggests that the high statistical significance of the heat flux-SST tendency correlations holds quite generally.

The principal conclusions that can be drawn from Table 1 are that (1) heat flux variability is controlled primarily by windspeed variability and (2) air temperature variability is a stronger controlling factor than SST. The sea-air temperature *difference* $SST - T_{Air}$ is what actually drives the fluxes (by Eq. 1), so the flux dependence on this difference is also shown in Table 1. Since the monthly means of SST and T_{Air} tend to fluctuate in phase, the $SST - T_{Air}$ difference tends to amplify the SST fluctuations and damp the T_{Air} fluctuations. This tendency is reflected in Table 1. It is noteworthy that by any measure given in Table 1, the SST tendency is better correlated with surface heat flux than is the SST itself. Both the U and C cases show very similar quantitative relationships between heat flux and the other fields.

For the U case, Fig. 8 shows the principal SVD "heterogeneous" correlation patterns in the heat flux field, or $r(\mathbf{S}, b_1)$, where $\mathbf{S}$ is the heat flux field and b_1 is the expansion coefficient of the first SVD mode for SST, air temperature, wind speed and SST tendency. The patterns are very similar in all cases, showing that increasing heat flux in the latitudes of weak mean winds are associated with decreasing heat flux over broad areas to the north and south, and with increasing flux over the southeast part of the basin. The similarity suggests that the patterns are dominated by a particular EOF of heat flux. This is indeed the case as illustrated by Fig. 9 which shows the first EOF of the surface heat flux. It explains 29% of the heat flux variability and has the same structure as the correlation patterns of Fig. 8. This structure is also found in the first wind speed EOF, but not for SST, air temperature and SST tendency. EOFs were computed (as were the SVD patterns) from the monthly mean time series with the seasonal cycle removed.

Figure 10 shows plots similar to Fig. 8 but for the C case. Qualitatively similar structures are observed for

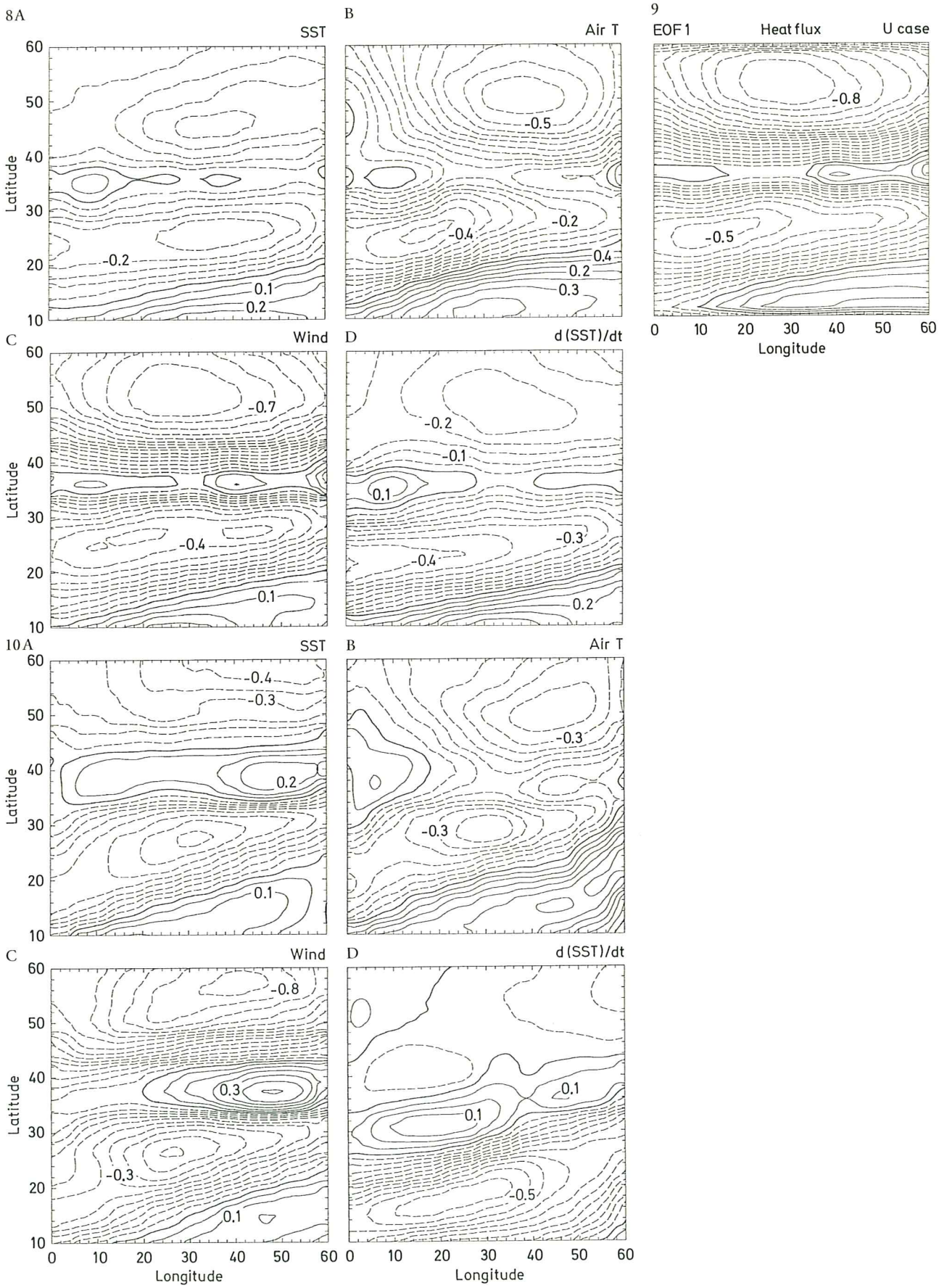
8A
SST
B
Air T
C
Wind
D
d(SST)/dt
10A
SST
B
Air T
C
Wind
D
d(SST)/dt
Latitude
Longitude
9
EOF 1
Heat flux
U case
Longitude

the heat fluxes associated with SST and wind speed (Fig. 10A, C). Patterns associated with SST tendency (Fig. 10D), however, are almost in quadrature with the patterns associated with SST and wind speed (Fig. 10A and 10C). As in the U case, these latter two patterns are dominated by the first EOF of heat flux, and have the characteristic southwest-northeast tilt. The correlation with air temperature (Fig. 10B) reflects the influence of the first air temperature EOF.

In summary, we are able to quantify how much the turbulent heat fluxes across the air-sea interface are controlled by each of the relevant atmospheric and oceanic state variables in both the coupled and uncoupled case. The patterns of heat flux correlation with SST and SST tendency are similar in the U case (Fig. 8A and 8D), yet show a quadrature relationship in the C case (Fig. 10A and 10D). The quadrature relationship is more intuitive, since it might be expected that where SST is at a maximum or minimum, SST tendency would be zero, and that where SST anomalies are close to zero, SST tendency would be strongly positive or negative. The difference between the U and C cases in this respect may simply reflect the greater ability of SST in the C case to resist changing in response to synoptic events in the atmosphere, since SST is itself influencing the atmosphere. In the C case the fact that air temperature covaries strongly with SST gives the ocean a greater effective thermal inertia. In the U case, on the other hand, SST is largely a slave to the atmosphere and effective thermal inertia is smaller. Heat fluxes associated with an SST higher than the month before (for a positive SST tendency) also tend to be associated with a positive SST anomaly.

4.2 SVD results for surface winds and SST tendency

In this subsection, SVD is used to investigate the systematic relationships between surface winds and SST tendency, since they are the fields that control the observed patterns of air-sea interaction according to the conceptual scenario of WSJ, as presented in Fig. 1. The atmospheric wind anomalies tend to be associated with either a "high-index" or "low-index" zonal flow regime. In the high-index case, zonal westerlies are stronger in mid-latitudes and zonal easterlies are stronger in the subtropics. These strong winds then lead to enhanced cooling in much of the ocean, with warming in the region between the westerlies and the trades. The warming was attributed by WSJ to the downwelling induced by the stronger zonal winds to the north and south. In the low-index regime, the sign of all anomalies was reversed, while the patterns remained the same. WSJ inferred the principal mode of air-sea interaction by computing temporal correlations between the principal EOFs of 500 mb geopotential height and both SST and SST tendency. Whereas correlations between 500 mb height and SST could not identify which field was forcing the other, correlations between 500 mb height and SST tendency could more easily be interpreted as atmospheric forcing of the ocean.

In this study, the interpretation of air-sea interactions is simpler as all the numerical experiments are performed in both uncoupled and coupled modes. This allows for a clean identification of those patterns which are due to atmospheric forcing of the ocean and likewise a clean identification of the effects of the coupling on those patterns. Furthermore SVD is a particularly well-suited statistical tool for identifying those principal patterns of interaction between an atmospheric and an oceanic field. The fact that the model geometry is generic implies that any teleconnections in the atmosphere, in the sense of Wallace and Gutzler (1981), are related to interaction with the ocean, since the atmospheric forcing is otherwise zonally symmetric: special characteristics of the Atlantic and Pacific are absent.

The schematic interaction presented by WSJ relates the strength of the atmospheric index cycle to heating and cooling in the ocean. Therefore, a SVD of the surface wind speed and SST tendency was performed, for both the U and C cases. A qualitative picture of the level of variability (and covariability) in each of these fields is presented in Fig. 11 which shows a 10-year segment from the 30-year time series of the first SVD expansion coefficients of wind speed and SST tendency for the C case. The correlation coefficient for the two tim series over the full 30 years is 0.58. Time series for the U case are similar.

Altough the heterogeneous correlation maps are orthogonal, a better physical understanding is gained by generating mean wind and SST tendency fields for those months when the first wind speed expansion coefficient (a_1) is greater than one standard deviation above its mean, and also for those months when the expansion coefficient is less than one standard deviation below its mean. Dimensional quantities are obtained rather than correlations. The *differences* between the above two mean fields are shown in Fig. 12. In both the U and C cases, a positive value of a_1 corresponds to a high index circulation, in which both the westerlies and the trades are stronger than normal. Conversely, negative a_1 corresponds to a low index circulation. The largest (positive) wind anomalies coincide with regions of enhanced SST cooling. In between these regions, weaker SST warming occurs under weak wind anomalies. Similar patterns are obtained if the data are stratified with the first SST tendency expansion coefficient (b_1) instead of the windspeed coefficient a_1.

Fig. 8A–D. Heterogeneous correlation patterns for the U case between the time series of the surface heat flux field and the first SVD expansion coefficient for **A** SST; **B** air temperature; **C** windspeed and **D** SST tendency. Contour interval is 0.05. Polarity of the fields is arbitrary

Fig. 9. EOF 1 of surface heat flux for the U case, shown as the correlation between (the time series of) the heat flux field and the expansion coefficient of the first EOF. Contour interval is 0.5

Fig. 10A–D. As in Fig. 8 but for the C case

11

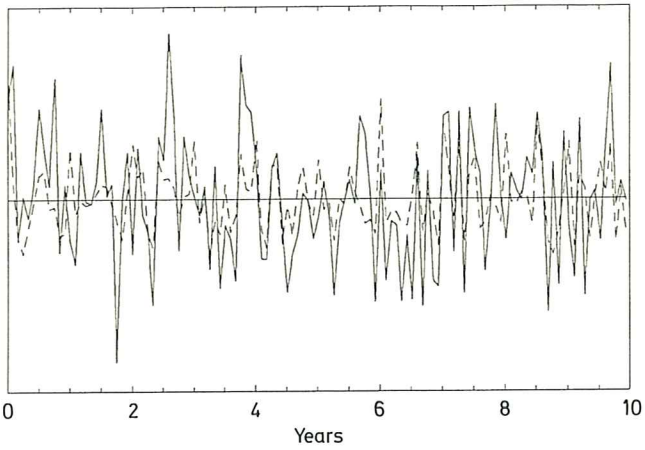
Wind and d(SST)/dt PC1 timeseries
C case
0
2
4
6
8
10
Years

12 A

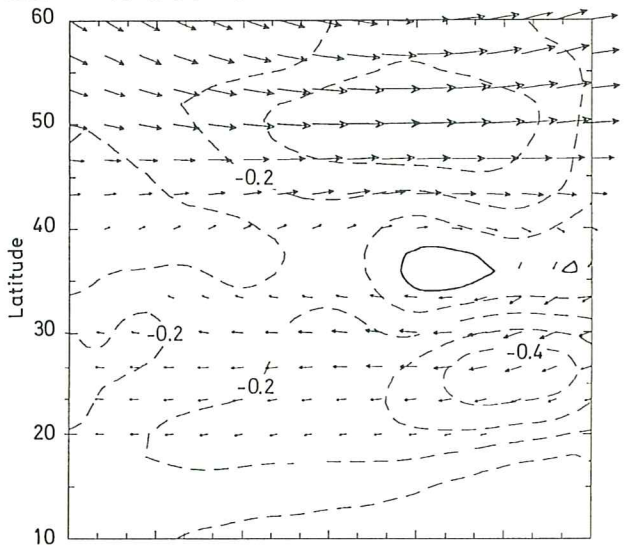
Hi-lo d(SST)/dt and wind differences
U case
60
50
40
30
20
10
Latitude
-0.2
-0.2
-0.4
-0.2

13 A

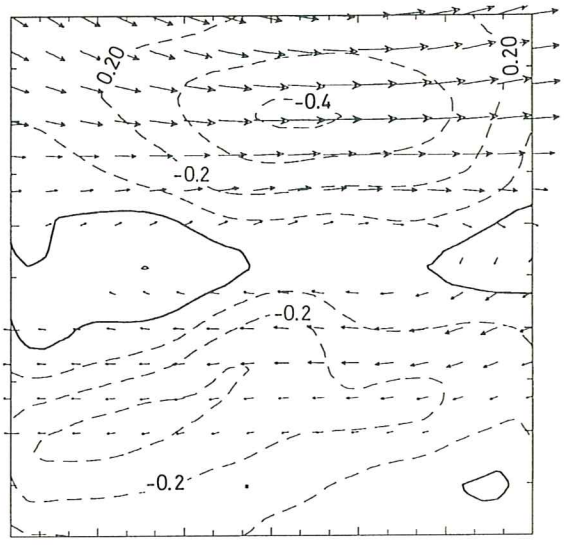
Hi-lo SST and wind differences
U case
0.20
0.20
-0.4
-0.2
-0.2
-0.2

B

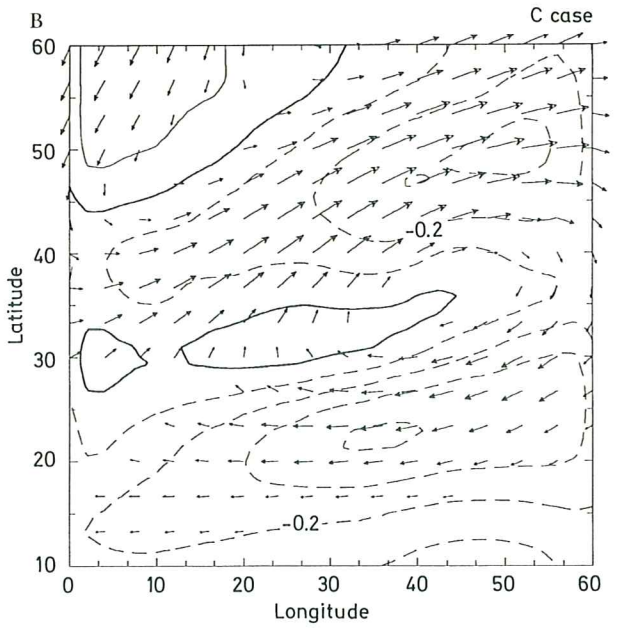
C case
60
50
40
30
20
10
Latitude
-0.2
-0.2
-0.2
0
10
20
30
40
50
60
Longitude

B

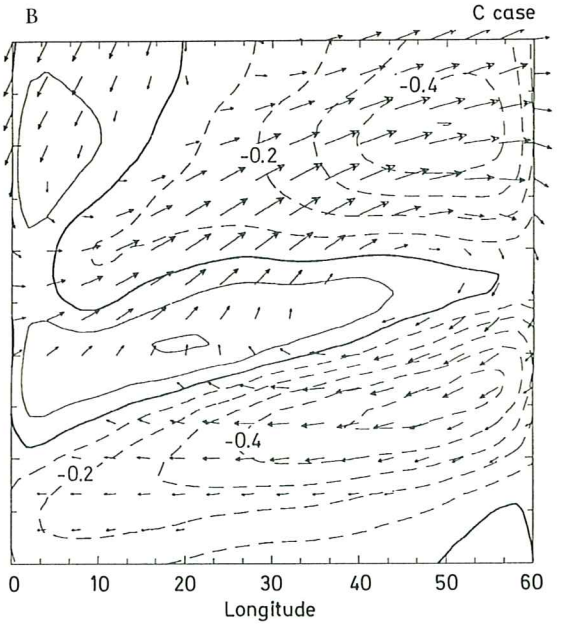
C case
-0.4
-0.2
-0.4
-0.2
0
10
20
30
40
50
60
Longitude

Figure 13 is identical to Fig. 12, except that SST differences are now shown between high and low values of a_1 instead of SST tendency differences. The underlying SVD remains between wind speed and SST tendency. Anomalously cool SST appears under anomalously strong winds in the westerly and easterly latitude belts, with anomalously warm SST in a narrow region in between. The patterns shown in Figs. 12 and 13 are robust and it makes virtually no difference if the data are stratified according to whether a_1 is positive or negative, or whether $|a_1|$ is greater than one standard deviation.

The contribution that the interaction mode makes to the total variability can be estimated by comparing the magnitudes of the interaction anomalies shown in Figs. 12 and 13 with the magnitudes of the standard deviations shown in Fig. 7. Near the centers of interaction approximately 20% of wind standard deviations and 10% of SST standard deviations are associated with coherent air-sea interaction. These estimates apply over localized areas, and a more rigorous quantitative estimate of the *global* variance explained by the interaction can be made from SVD of wind speed and SST tendency. For the U case, it is found that 4.3% of the wind speed variance could be accounted for by covariance with the first SVD expansion coefficient of the SST tendency. Similarly, 3.9% of the variance in SST tendency is explained by the first expansion coefficient of the wind speed. Corresponding numbers for the C case are 5.6% and 5.4% respectively. While these percentages appear to be low, significance tests in fact indicate that they are highly significant. Statistical significance was evaluated as in subsection 4.1 using a Monte Carlo data scrambling method. In both the U and C cases, the time series sequence of the wind speed field (the dominant of the two fields) was randomly scrambled. In none of the scrambled cases was more than 1% of wind speed variance explained by the first expansion coefficient of SST tendency. At most, only 0.7% of variance in SST tendency was accounted for by the first wind speed expansion coefficient. It is reasonable, then, to conclude that at least 80% of whatever variance in one field is "explained" by the singular values in another is explained by a real physical connection, and less than 20% is due to statistical accident.

In the results shown here, the 30-year mean seasonal cycle was removed from the data before performing the SVD and EOF calculations. However the *effect* of the annual cycle still remains in the form of significantly higher variability in all dynamical fields during winter time. Most of the observational studies referred to in this paper (such as WSJ) used data based on seasonal means. The analyses presented are based on 30 years of year-round, monthly mean fields. They were repeated for completness using 30 years of winter time (Dec.–Feb.) seasonal-mean fields. The *patterns* obtained with this data set are very similar to those presented for the monthly mean data, with the notable exception that patterns involving SST tendency more closely resembled the analogous patterns involving SST. *Quantitatively,* however, air-sea interaction explained much more of the variance in each field than it did for the monthly mean data. The most dramatic example of this is in the SVD analysis comparing wind speed and SST tendency. The amount of wind speed variability in the coupled model explained by the first SVD expansion coefficient of SST tendency increased from 5.7% using monthly-mean data to 19.1% using winter-mean data.

Table 2 shows the same quantities as Table 1, but for the winter-mean data set, and for the C case only. In general, the winter-mean time series shows the signal of air-sea interaction standing out better from the noise of other dynamical processes in the atmosphere and ocean. The numbers shown in Table 2 reflect a signal-to-noise ratio comparable in magnitude to that found in the observations by WSJ and WSB. We have not emphasized the use of this shorter winter-mean time series in this study because significant air-sea interactions occur on monthly (or shorter) time scales, as is evident in Fig. 11. Calculations were also performed using instantaneous fields sampled every 10 days from both the ocean and atmosphere. Again, the patterns found were very similar to those shown here while quantitatively the numbers all decreased from those shown in Table 1.

In summary, Figs. 12 and 13 represent a strong confirmation of the schematic picture presented by WSB and in Fig. 1. Basin-scale air-sea interaction is controlled by the dominant "index cycle" pattern of variability in the atmosphere. In the high-index phase of this cycle, anomalously strong mid-latitude westerlies and subtropical easterlies enhance heat flux out of the ocean, leading to strong SST cooling in those latitudes, with weaker heating in the region in between. All signs are reversed in the low-index (or weak zonal wind) phase of the cycle. The effect of the SST feedback onto the atmosphere is principally to orient and localize the anomalies. This interaction mechanism is robust; very

Fig. 11. The first 10 years of the time series of the expansion coefficients of the windspeed (a_1; *solid*) and SST tendency (b_1; *dahsed*) from the first SVD mode in the C case. The correlation coefficient between these two time series over 30 years ($r(a_1, b_1)$) is 0.54. Ordinate scaling is arbitrary; the zero line is shown

Fig. 12A, B. Difference fields for SST tendency (*contours*) and surface winds (*arrows*) between the mean fields corresponding to values of a_1 larger than one standard deviation above its mean and the mean fields corresponding to values of a_1 less than one standard deviation below its mean. These fields show one polarity of the principal pattern of covariability between the surface winds and SST tendency, as stratified by projection of the first wind speed singular vector onto the wind field (a_1). The U case is shown in **A**, the C case in **B**. SST tendency differences are contoured every 0.1° C month^{-1}, with *negative contours dashed.* The *largest arrow* represents wind speed differences of 3.4 ms^{-1} in **A** and 2.4 ms^{-1} in **B**; wind differences less than 0.5 ms^{-1} are not shown

Fig. 13A, B. Difference fields as in Fig. 12, but for surface winds and SST (rather than SST tendency). The U case is shown in **A**, the C case in **B**. SST differences are contoured every 0.1° C, with *negative contours dashed. Wind arrows* are as in Fig. 12

Table 2. SVD results as in Table 1, but for the C case only, and based on the 30-year winter-mean time series rather than the 360-sample time series of monthly means

	$\|C_{ST}\|_F$	$\langle r(S, b_{1:2:6})^2 \rangle$
SST	0.22	11.9 18.3 32.4
T_{Air}	0.20	14.2 23.1 45.2
SST-T_{Air}	0.19	13.4 24.2 50.7
WIND	0.36	20.9 36.0 72.5
d(SST)/dt	0.31	20.7 38.7 69.9

similar patterns were obtained from datasets consisting of monthly means, seasonal-means and instantaneous fields every 10 days. The interaction is most dominant in the seasonal-mean data, where there are relatively few other processes inducing variability on such a time scale, but its natural time scale is considerably shorter than this. Hence the focus on the monthly mean dataset in this paper.

5 Discussion and conclusions

The characteristic patterns of large-scale air-sea interaction in midlatitudes and the relationships between the different physical parameters involved have been investigated using numerical models. The models are a 6-layer isopycnic-coordinate model of a mid-latitude ocean basin and a 2-layer global spectral model of the atmosphere. They have been integrated synchronously in both uncoupled and coupled modes. In the uncoupled case, the atmosphere only feels the ocean climatology, but in the coupled case feels the fully time-varying ocean. There is no climate drift: statistically stationary climates were obtained for the upper ocean and atmosphere in both cases. The fact that the coupled model equilibrates and has no continuous climate drift is probably not remarkable given that radiative equilibrium is restored in the atmosphere by a Newtonian cooling-type relaxation, which is less tolerant of climate drift than a direct forcing would be. Time-mean and variance fields in the coupled model have more zonal structure but are still comparable to those in the uncoupled case.

Surface heat fluxes were used as the primary measure of air-sea interaction, and the covariability of these fluxes with SST, air temperature, surface wind speed and SST tendency was investigated using SVD and EOF analyses. In the model, heat flux is an explicit nonlinear function of SST, air temperature and wind speed. The analyses indicate that the heat flux is primarily controlled by the wind speed and that it is more closely related to air temperature and SST tendency than it is to SST itself. The dominant patterns of covariability have generic features, such as a zonal elongation with a slight southwest-northeast tilt, and a "sandwich"-like structure in the meridional.

Air-sea interaction patterns show both qualitative and quantitative similarity between the uncoupled and coupled cases, indicating that atmospheric forcing of the ocean is dominant in the interactions. The ocean is not a completely passive player, however, and plays a significant role in organizing the interactions into geographically localized regions, as is evident from Figs. 12 and 13.

These model results lend further support and explanation to the notion that the principal mode of large-scale air-sea interaction in mid-latitudes is a coherent oceanic response to index-cycle variability in the atmosphere. Anomalous winds tend to either strengthen or weaken both the mid-latitude westerlies and the subtropical trades. Stronger winds strip heat out of the underlying ocean, decreasing the SST. Any feedback from the ocean to the atmosphere will then be negative, since cooler SST will tend to weaken the warm-core anti-cyclone that gave rise to the initial positive wind anomalies. This negative feedback is one possible reason why air-sea interaction in mid-latitudes has a much weaker climatic signature than air-sea interaction in the tropics.

Acknowledgement. This research was funded by the U.S. Department of Energy's (DOE) National Institute for Global Environmental Change (NIGEC) through the NIGEC Southeast Regional Center at the University of Alabama, Tuscaloosa. (DOE Cooperative Agreement No. DE-FC03-90ER61010.) Financial support does not constitute an endorsement by DOE of the views expressed in this paper.

Appendix

Following the notation of Bretherton et al. (1992), we choose one field (e.g., the time series of heat fluxes at each ocean gridpoint) as the "left" data field $\mathbf{l}(\mathbf{S}, t)$. The "right" data field $\mathbf{T}(\mathbf{x}, t)$ is chosen to be the time series of another variable (e.g., SST) at the same set of points[1]. The correlation matrix C_{ST} is then constructed from temporal correlations between the heat fluxes at each gridpoint and SST at each gridpoint; i.e.,

$$C_{ST} = \langle \mathbf{S}(t)\mathbf{T}^T(t) \rangle, \tag{2}$$

where the angle brackets represent a time average, and superscript T signifies a transpose. Since an equal number of points ($N = 32^2 = 1024$) are used for both fields, C_{ST} is an $N \times N$ matrix.

SVD is then defined by the following unique matrix decomposition:

$$C_{lr} = \sum_{k=1}^{R} \sigma_k \mathbf{l}_k \mathbf{r}_k^T, \quad R \leq N \tag{3}$$

[1] It is not necessary, however, to have the left and right fields defined at the same set of points

Here the $\mathbf{l}_k$ and $\mathbf{r}_k$ are two orthonormal sets of R vectors of length N called the left and right singular vectors, respectively. The σ_k are nonnegative numbers called singular values and are ordered such that $\sigma_1 \geq \sigma_2 \ldots \geq \sigma_R$, and R is the rank of C_{ST}.

The heat flux field at each time can be projected onto each of the left singular vectors to produce a time series of expansion coefficients $a_k(t)$ for each singular vector $\mathbf{l}_k$. Time series of expansion coefficients b_k for each right singular vector may be found similarly:

$$a_k(t) = \mathbf{l}_k^T \mathbf{S}(t), \; b_k(t) = \mathbf{r}_k^T \mathbf{T}(t). \tag{4}$$

At each time the heat flux field can be approximated by a linear combination of the orthonormal patterns $\mathbf{l}_k$, and the other (e.g., SST) field can be approximated by a linear combination of the orthonormal patterns $\mathbf{r}_k$:

$$\mathbf{S}(t) \simeq \sum_{k=1}^{R} a_k(t)\,\mathbf{l}_k, \tag{5}$$

$$\mathbf{T}(t) \simeq \sum_{k=1}^{R} b_k(t)\,\mathbf{r}_k. \tag{6}$$

In the expansion of the original fields into sums of orthonormal patterns, the leading singular vectors or patterns $\mathbf{l}_1$ and $\mathbf{r}_1$ have the property that the projection $a_1(t)$ of $\mathbf{S}$ onto $\mathbf{l}_1$ has the maximum correlation with the projection $b_1(t)$ of $\mathbf{T}$ onto $\mathbf{r}_1$; i.e.,

$$\langle a_1(t), b_1(t) \rangle = \max = \sigma_1 \tag{7}$$

Successive pairs of patterns $(\mathbf{l}_k, \mathbf{r}_k)$ each explain the next largest correlation, subject to the condition that $\mathbf{l}_k$ is orthogonal to $\mathbf{l}_{-1}, \ldots, \mathbf{l}_{k-1}$, and $\mathbf{r}_k$ is orthogonal to $\mathbf{r}_1, \ldots, \mathbf{r}_{k-1}$.

The sum of the squares of each entry in C_{ST}, normalized by the total number of entries, is equal to the total squared correlation between the two fields and is defined to be the square of the Frobenius norm of C_{ST}, or $\|C_{ST}\|_F^2$. In SVD, the square of this norm of C_{ST} is proportional to the sum of the squares of its singular values:

$$\|C_{ST}\|_F^2 = N^{-2} \sum_{k=1}^{R} \sigma_k^2 \tag{8}$$

The cumulative squared correlation fraction ($CSCF$) of C_{ST} accounted for by the leading n modes is defined as

$$CSCF_n = \frac{\sum_{k=1}^{n} \sigma_k^2}{\sum_{k=1}^{R} \sigma_k^2} \tag{9}$$

Our interest is naturally drawn to those singular vectors whose singular values explain large fractions of the total squared correlation between the two fields. Results are presented graphically in the form of "left" and "right" heterogeneous correlation maps, defined by $r[\mathbf{S}(t), b_k(t)]$ and $r[\mathbf{T}(t), a_k(t)]$, respectively. Since our time series are normalized, the left and right heterogeneous maps are proportional to the left and right singular vectors, respectively, and are mutually orthogonal in space. The heterogeneous maps for the kth mode in the SVD expansion provide a measure of how well the anomaly patterns in the "right" field (T) are explained by the kth expansion coefficient of the heat flux field (S) and vice versa. Homogeneous correlation maps, on the other hand, defined by $r[\mathbf{S}(t), a_k(t)]$ and $r[\mathbf{T}(t), b_k(t)]$, are not proportional to any singular vector and are not mutually orthogonal.

References

Bjerknes J (1964) Atlantic air-sea interaction. Adv Geophys 20:1–82

Bleck R, Hanson HP, Hu D, Kraus EB (1989) Mixed layer/thermocline interaction in a three-dimensional isopycnal model. J Phys Oceanogr 19:1417–1439

Bretherton CS, Smith C, Wallace JM (1992) An intercomparison of methods for finding coupled patterns in climate data. J Clim 5:541–560

Cayan DR (1992a) Latent and sensible heat flux anomalies over the Northern Oceans: the connection to monthly atmospheric circulations. J Clim 5:354–369

Cayan DR (1992b) Latent and sensible heat flux anomalies over the Northern Oceans: driving the sea surface temperature. J Phys Oceanogr 22:859–881

Frankignoul C (1985) Sea surface temperature anomalies, planetary waves and air-sea feedback in the middle latitudes. Rev Geophys 23:357–390

Kraus EB, Turner JS (1967) A one-dimensional model of the seasonal thermocline: II. The general theory and its consequences. Tellus 19:98–106

Hellerman S, Rosenstein M (1983) Normal monthly wind stress over the world ocean with error estimates. J Phys Oceanogr 13:1093–1104

Lanzante JR (1984) A rotated eigenanalysis of the correlation between 700 mb heights and sea surface temperatures in the Pacific and Atlantic. Mon Weather Rev 112:2270–2280

Manabe S, Stouffer RJ (1988) Two stable equilibria of a coupled ocean-atmosphere model. J Clim 1:841–866

Manabe S, Stouffer RJ, Spelman MJ, Bryan K (1991) Transient responses of a coupled ocean-atmosphere model to gradual changes of atmospheric CO_2. Part I: annual mean response. J Clim 4:785–818

Miller AJ, Roads JO (1990) A simplified coupled model of extended-range predictability. J Clim 3:523–542

Namias J, Cayan DR (1981) Large-scale air-sea interactions and short-period climatic fluctuations. Science 214:869–876

Namias J, Yuan X, Cayan DR (1988) Persistence of North Pacific sea surface temperature and atmospheric flow patterns. J Clim 1:682–703

Peixoto JP, Oort AH (1992) Physics of Climate. American Institute of Physics 520 pp

O'Brien E, Stewart DA, Branscome LE (1994) Tropical-extratropical interactions on intraseasonal time scales in a global spectral model. J Atmos Sci 51:1244–1260

Palmer TN, Sun ZB (1985) A modeling and observational study of the relationship between sea surface temperature in the northwest Atlantic and the atmospheric general circulation. Q J R Meteorol Soc 111:947–975

Sausen R, Barthel K, Hasselmann K (1988) Coupled atmosphere models with flux correction. Clim Dyn 2:145–163

Wallace JM, Gutzler DS (1981) Teleconnections in the geopotential height field during the northern hemisphere winter. Mon Wea Rev 109:784–812

Wallace JM, Smith C, Jiang Q (1990) Spatial patterns of Atmosphere-Ocean interaction in the Northern Winter. J Clim 3:990–998

Wallace JM, Smith C, Bretherton CS (1992) Singular value decomposition of wintertime sea surface temperature and 500 mb height anomalies. J Clim 5:561–576